Dynamic plasma response in laser-photodetachment experiments in hydrogen plasmas

L. Friedland,* C. I. Ciubotariu, and M. Bacal
Laboratoire de Physique des Milieux Ionises, Laboratoire du C.N.R.S., Ecole Polytechnique, 91128 Palaiseau, France
(Received 15 September 1993)

The theory of the dynamic plasma response in laser-photodetachment experiments in low pressure hydrogen plasmas is extended to include the effects of the self-consistent electric field. The H^- rich plasma is modeled via a hybrid fluid-kinetic approach in which the electrons and positive ions are described by the fluid theory, while the negative ions are treated within the ballistic kinetic theory. Both slab and cylindrical geometries of the plasma region illuminated by the laser are analyzed. The model is applied for studying the space-time evolution of various plasma species after the photodetaching laser pulse. The experimentally observed overshoot in the time dependence of the electron density perturbation on the axis or plane of symmetry was analyzed in detail. The overshoot is due to the depletion of the positive ions as the result of the self-consistent electric field. The magnitude of the overshoot and the time of the maximum depletion of the positive ions are sensitive to the ratio between the electron and positive ion temperatures.

PACS number(s): 52.40.Nk, 51.10.+y, 51.50.+v, 52.70.−m

I. INTRODUCTION

Low pressure hydrogen isotope plasmas (referred to as negative ion plasmas in the following) are proposed as sources for the production of neutral beams for use in the next generation of large tokamaks [1]. These ambitious plans are based on the extensive experimental and theoretical effort invested in the research and development of these sources in the last two decades [2]. Nevertheless, a further effort is needed in developing sources for more demanding future applications. Therefore, the development of new and reliable diagnostic techniques and the subsequent characterization of the negative ion plasmas is one of the main goals of the current and future experiments.

One of the important diagnostic tools for studying negative ion plasmas is based on the laser-photodetachment technique [3], in which one rapidly destroys the negative ions in a certain region in the plasma by an intense laser light, and studies the plasma response by probe measurements. These experiments served, in the past, to determine negative ion densities and temperatures in a variety of plasma configurations [4–6] providing important information for checking and further developing our theoretical understanding of the physical processes involved in negative ion sources. It should be mentioned that the theoretical modeling of these sources is, in principle, a difficult task, since the plasmas are weakly collisional and only partially confined.

The goal of this work is to advance our theoretical understanding of the dynamics of evolution of various plasma components in the laser-photodetachment experiments in searching for new means of diagnostics of H^- or D^- plasmas. Presently, the theory of the laser-photodetachment method [5] neglects the ambipolar electric field induced in the plasma by a local increase δn^e of the electron density immediately following the laser pulse. Thus, one treats the problem of the return of the negative ion density n^- to its steady-state value n_0^- by using a simple *ballistic* kinetic theory. This approach was very successful in studying the negative-ion evolution for times of order $R/v_{\rm th}^-$, where R and $v_{\rm th}^-$ are the radius of the cylindrical region in the plasma affected by the laser beam and the thermal velocity of the negative ions. However, for other plasma species and at later times, certain experimental details remained unexplained by the ballistic theory. For example, Fig. 1 (see Ref. [4]) shows a typical experimental evolution of n^-/n_0^- for the H^- ions (the full circles) and of the relative electron density perturbation $\delta n^e/n_0^-$ (the open circles) on the axis of the illuminated plasma region. The electron density, in these experiments, was determined from the electron current to a positively biased probe located on the axis, while the H^- density is deduced from a more complex procedure, involving the utilization of the second laser pulse [4–6]. The experiments show that for times of the order of $R/v_{\rm th}^-$ the time dependence of n^-/n_0^- on the axis was of the form $n_0^- \exp[-(R/tv_{\rm th}^-)^2]$. This dependence was also predicted by the ballistic model [5] assuming a Maxwellian negative ion velocity distribution. On that basis, the above experiments allowed systematic negative ion temperature measurements. Nevertheless, we can see in Fig. 1 that, while the H^- density return to equilibrium is described by a simple monotonically increasing law, the electron density evolves in a more complex fashion and has a characteristic overshoot at some time. By assuming quasineutrality, this difference can be explained

*On sabbatical from the Center of Plasma Physics, Racah Institute of Physics, Hebrew University of Jerusalem, Jerusalem, Israel.

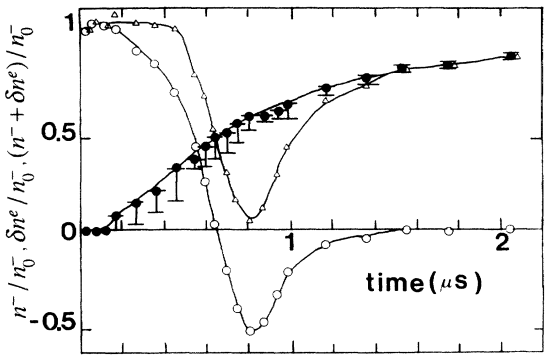

FIG. 1. Typical experimental time dependence [4] of the normalized negative ion density n^-/n_0^- (full circles) and normalized electron density perturbation $\delta n^e/n_0^-$ (open circles) after the laser-induced photodetachment. The sum $(n^- + \delta n^e)/n_0^- = \delta n^+/n_0^- + 1$ (triangles) describes the expected evolution of the normalized (and shifted by 1) positive ion density perturbation.

[4] by the departure of the positive ions from equilibrium. This effect is illustrated in Fig. 1 by the sum $(\delta n^e + n^-)/n_0^-$ (shown by triangles in the figure) of the electron and negative ion curves. Due to the quasineutrality this sum is equal to $\delta n^+/n_0^- + 1$, where δn^+ is the expected positive ion density perturbation. But the positive ions, initially unaffected by the laser light, can only move due to the ambipolar electric field, and thus this field is important for explaining all the details in Fig. 1.

In the present work we advance the theory of laser-photodetachment experiments in H^- plasmas. Our approach will still be based on the ballistic kinetic theory for the negative ions, since, previously, this approach was successful in interpreting the H^- density evolution. Nevertheless, we shall include the effect of the electric field on the electrons and the positive ions, by treating these two species within a *fluid* model consistent with the *kinetic* evolution of the H^- ions. Thus we shall develop a complete *hybrid fluid-kinetic* picture of plasma dynamics in laser-photodetachment experiments in negative ion plasmas.

II. HYBRID FLUID-KINETIC MODEL

Consider a collisionless, uniform, three-species plasma [5] electrons, (H^-, H_3^+), where at some time ($t=0$) one illuminates a cylindrically symmetric region by a fast (on the ion acoustic time scale) intense laser pulse. As the result of the photodetachment, one thus destroys (fully or partially) H^- ions, creating a local electron density increase $\delta n^e(r,t=0) \equiv \Delta(r)$ and a corresponding depletion $\delta n^-(r,t=0) \equiv -\Delta(r)$ in the negative ion density (r measures the distance from the axis of the illuminated region). We are interested in calculating the plasma response to this perturbation for $t>0$. We shall limit our analysis to plasmas in which the negative ions comprise the minority species, i.e., before the laser pulse, $(n^-/n^e)_{t<0} \equiv n_0^-/n_0^e \ll 1$, and, thus, $(n^e/n^+)_{t<0} \equiv n_0^e/n_0^+ \approx 1$. Furthermore, we shall discuss the evolution on the slow, ion acoustic time scale $\Delta t \sim R/v_a$ (R being the radius of the illuminated region and v_a the characteristic ion acoustic speed). Therefore, the details of the initial plasma oscillations on the electron plasma frequency time scale $\Delta t \sim \omega_p^{-1}$ are outside the scope of this work. Finally, we observe that, while by assumption the relative initial perturbations of the electron and positive ion densities due to the laser pulse are small or even zero (for H_3^+), the relative change of the negative ion density is large, as all negative ions may be destroyed by a sufficiently intense laser pulse [3] creating a large density gradient at the edge of the illuminated plasma region. Therefore, we shall treat the electrons and positive ions within the linearized fluid model, but use a kinetic description for the negative ion species.

We proceed by writing the linearized continuity and momentum equations for H_3^+,

$$\partial_t(\delta n^+) + n_0^+ \partial_r(\delta v^+) = 0 , \tag{1a}$$

$$M^+ \partial_t(\delta v^+) = -e\partial_r(\delta\phi) - (\gamma k_B T^+/n_0^+)\partial_r(\delta n^+) , \tag{1b}$$

where δn^+ and δv^+ are the positive ion density perturbation and the radial fluid velocity, M^+ and T^+ are the positive ion mass and temperature, $\gamma=3$ is the adiabatic index, e is the electron charge, and k_B is the Boltzmann constant. The variable $\delta\phi$ in (1) is the self-consistent radial potential, created in the plasma due to the nonuniformity and the finite electron temperature. This potential confines the electrons, so for the perturbed electron density we use the linearized Boltzmann law

$$\delta n^e = n_0^e(e\delta\phi/k_B T^e) , \tag{2}$$

where T^e is the electron temperature. Instead of the Poisson equation for $\delta\phi$, for simplicity, we use the plasma approximation

$$\delta n^+ = n^- - n_0^- + \delta n^e , \tag{3}$$

thus limiting the discussion to nonuniformity scales large compared to the Debye length. Finally, we employ the kinetic description (see the discussion above), i.e., use the ballistic approximation in the Vlasov equation for the distribution function f^- of the negative ions:

$$(\partial_t + \mathbf{v}\cdot\partial_r) f^- = 0 . \tag{4}$$

In other words, we neglect the term $-e\mathbf{E}\cdot\partial_v f^-$ [$\mathbf{E}$ being the electric field $-\partial_r(\delta\phi)$]. The ballistic approximation was already used successfully in describing some of the results of the photodetachment experiments [5,6]. The negative ion temperature T^- found in these experiments was sufficiently high so that the velocities of the majority of the negative ions are only slightly perturbed by the potential $\delta\phi$ and, to a good approximation, one can neglect this effect. The formal validity condition for the ballistic approximation is $e\delta\phi/k_B T^- \ll 1$ and we shall see later that this condition is satisfied in our case, provided $T^- \sim O(T^e)$. The knowledge of f^- from (4) allows one to calculate the negative ion density variation

$$\Delta n^- \equiv n^- - n_0^- = \int (f^- - f_0^-) d^3v \tag{5}$$

for any given initial distribution $f_0^-(\mathbf{v})$, so we have a closed set of equations describing our problem. Finally, we specify the initial conditions. In accordance with the experimental conditions described above, we use zero initial conditions for δn^+, δv^+, but

$$(f^- - f_0^-)_{t=0} = -f_0^-(\mathbf{v})\Delta(r)/n_0^- \neq 0 \ . \tag{6}$$

We solve our linear, initial value problem via Fourier transform in space and Laplace transform in time. Consequently, say for $\Delta f^-(\mathbf{v},\mathbf{r},t) \equiv f^-(\mathbf{v},\mathbf{r},t) - f_0^-(\mathbf{v})$, we introduce the Fourier-Laplace transform

$$\Delta F^-(\mathbf{v},\mathbf{k},\omega) \equiv (2\pi)^{-2} \int_{-\infty}^{+\infty} d^2r \int_0^{\infty} \Delta f^-(\mathbf{v},\mathbf{r},t) \times \exp(i\omega t - i\mathbf{k}\cdot\mathbf{r}) dt , \tag{7}$$

where $\mathbf{k}$ is a two-dimensional real vector and $\mathrm{Im}\omega > 0$. Similarly, we transform all the rest of the dependent variables and denote the transformed variables by capital letters. The resulting system for the transformed variables is

$$-i\omega(\delta N^+) + in_0^+ \mathbf{k}\cdot(\delta \mathbf{V}^+) = 0 \ , \tag{8a}$$

$$-i\omega M^+(\delta \mathbf{V}^+) = -i\mathbf{k}e(\delta\Phi) - (\gamma k_B T^+/n_0^+) i\mathbf{k}(\delta N^+) \ , \tag{8b}$$

$$\delta N^+ = \Delta N^- + \delta n^e = \Delta N^- + n_0^e(e\delta\Phi/k_B T^e) \ , \tag{8c}$$

$$\Delta N^- = \int \Delta F^- d^3v \ , \tag{8d}$$

$$-i(\omega - \mathbf{k}\cdot\mathbf{v})\Delta F^- = \Delta f^-(0,\mathbf{k}) \ , \tag{8e}$$

where

$$\Delta f^-(0,\mathbf{k}) \equiv (2\pi)^{-2} \int_{-\infty}^{+\infty} \Delta f^-(\mathbf{v},\mathbf{r},t=0) \times \exp(-i\mathbf{k}\cdot\mathbf{r}) d^2r = -(2\pi)^{-2}[f_0^-(\mathbf{v})/n_0^-]\delta n^e(\mathbf{k},0) \tag{9}$$

is the Fourier transform of the initial change of the negative ion distribution induced by the laser pulse [see Eq. (6)] and

$$\delta n^e(\mathbf{k},0) \equiv \int_{-\infty}^{+\infty} \Delta(r)\exp(-i\mathbf{k}\cdot\mathbf{r}) d^2r = (2\pi)^{-1} \int_0^{\infty} r\Delta(r) J_0(kr) dr \tag{10}$$

is the Fourier transform of the initial electron density perturbation.

The further steps are simple. First, we substitute ΔF^- from Eq. (8e) into Eq. (8d), yielding

$$\Delta N^- = i[\delta n^e(\mathbf{k},0)/n_0^-] \int f_0^-(\mathbf{v})(\omega - \mathbf{k}\cdot\mathbf{v})^{-1} d^3v \ . \tag{11}$$

Limiting the discussion to the Maxwellian $f_0^-(\mathbf{v}) = (\pi^{1/2} v_{\mathrm{th}}^-)^{-3} n_0^- \exp[-(v_x^2 + v_y^2 + v_z^2)/(v_{\mathrm{th}}^-)^2]$ for the negative ions, choosing (for given $\mathbf{k}$) the x axis along $\mathbf{k}$, and integrating in (11) over v_y and v_z, we obtain

$$\Delta N^- = i(\pi^{1/2} v_{\mathrm{th}}^-)^{-1} \delta n^e(\mathbf{k},0) \times \int_{-\infty}^{+\infty} \exp[-(v^2/v_{\mathrm{th}}^-)^2](\omega - kv)^{-1} dv \ . \tag{12}$$

Next, we use Eqs. (8a) and (8b) to find

$$N^+ = (en_0^+ k^2/M^+)[\omega^2 - k^2(v_{\mathrm{th}}^+)^2]^{-1} \delta\Phi \ , \tag{13}$$

where $(v_{\mathrm{th}}^+)^2 = \gamma k_B T^+/M^+$. Then, the use of (12) and (13) in (8c) yields

$$\delta\Phi(\mathbf{k},\omega) = -i(\pi^{1/2} v_{\mathrm{th}}^-)^{-1}(k_B T^e/e)[\delta n^e(\mathbf{k},0)/n_0^e] \times \int_{-\infty}^{+\infty} \frac{\omega^2 - k^2(v_{\mathrm{th}}^+)^2}{\omega^2 - k^2 v_a^2} \frac{\exp[-(v/v_{\mathrm{th}}^-)^2]}{\omega - kv} dv \ , \tag{14}$$

where, as usual, the ion acoustic speed is defined via $v_a^2 = (v_{\mathrm{th}}^+)^2 + k_B T^e/M^+$.

Next, we invert the Laplace transform in Eq. (14), i.e., find $\delta\phi(\mathbf{k},t) = (2\pi)^{-1} \int_{-\infty+i\sigma}^{+\infty+i\sigma} \exp(-i\omega t)\delta\Phi(\mathbf{k},\omega) d\omega$, where $\sigma > 0$. The integration is performed by closing the integration contour in the lower complex ω plane and using the residue theorem. This yields the image of the potential in the Fourier space

$$\delta\phi(\mathbf{k},t) = -(\pi^{1/2} v_{\mathrm{th}}^-)^{-1}(k_B T^e/e)[\delta n^e(\mathbf{k},0)/n_0^e] \times \int_{-\infty}^{+\infty} \frac{[v_a^2 - (v_{\mathrm{th}}^+)^2]\cos(kv_a t) - [v^2 - (v_{\mathrm{th}}^+)^2]\cos(kvt)}{v_a^2 - v^2} \exp[-(v/v_{\mathrm{th}}^-)^2] dv \ . \tag{15}$$

By inverting the Fourier transform in (15), we find the desired solutions $\delta\phi(r,t)$ and $\delta n^e(r,t)$:

$$\delta n^e(r,t)/n_0^e = e\delta\phi(r,t)/k_B T^e = 2(n_0^-/n_0^e)(\pi^{1/2} v_{\mathrm{th}}^-)^{-1} \int_0^{+\infty} \frac{[v_a^2 - (v_{\mathrm{th}}^+)^2]\Psi(r,v_a t) - [v^2 - (v_{\mathrm{th}}^+)^2]\Psi(r,vt)}{v_a^2 - v^2} \exp[-(v/v_{\mathrm{th}}^-)^2] dv \ , \tag{16}$$

where the function Ψ is given by

$$\Psi(r,a)=\int d^2k[\delta n^e(\mathbf{k},0)/n_0^-]\cos(ka)$$
$$=2\pi\int_0^\infty k\,dk[\delta n^e(k,0)/n_0^-]\cos(ka)J_0(kr) \tag{17}$$

and J_0 is the Bessel function of the first kind. By substituting the definition of $\delta n^e(k,0)$ [see Eq. (10)] we can also write

$$\Psi(r,a)=\int_0^\infty r'dr'\int_0^\infty k\,dk[\Delta(r')/n_0^-]\cos(ka)$$
$$\times J_0(kr)J_0(kr')\ . \tag{18}$$

A procedure similar to the above can be used to find the negative ion density [Eq. (11)]:

$$\delta n^-(r,t)/n_0^-=-2(\pi^{1/2}v_{\rm th}^-)^{-1}$$
$$\times\int_0^{+\infty}\Psi(r,vt)\exp[-(v/v_{\rm th}^-)^2]dv\ . \tag{19}$$

Note that the same result can be obtained directly from (16), by substituting $v_a=v_{\rm th}^+$. In this case $T^e=0$ and, therefore, no potential is induced in the plasma, the positive ions remain stationary, so $\delta n^-(r,t)=-\delta n^e(r,t)$. Finally, when δn^- and δn^e are known, the positive ion density can be found by using quasineutrality. This completes the formal solution of our problem.

We conclude this section with the following remarks. First, we note that the integrand in (16) is, generally, not singular, since at $v=v_a$ we can replace the factor multiplying the exponent in the integrand by $(2v_a)^{-1}(\partial/\partial v)\{[v^2-(v_{\rm th}^+)^2]\Psi(r,vt)\}_{v=v_a}$. Therefore, only in the case of a singular derivative of Ψ is the integrand singular. Second, the small factor n_0^-/n_0^e in (16) provides the *a posteriori* justification of the ballistic assumption for the negative ions and shows that the self-consistent potential in the plasma is small if the initial fraction of the negative ions in the plasma is small. The inverse argument shows that, if n_0^-/n_0^e is of the order of 1 or larger and $T^-\sim O(T^e)$, one cannot use the ballistic theory and must take into account the effect of the electric field on the negative ions. Third, we observe that the initial Maxwellian distribution of the H^- ions in our theory can easily be replaced by any other isotropic, normalized distribution function $f_0^-(v^2)[4\pi\int_0^\infty f_0^-(v^2)v^2dv=1]$. This would only require the replacement of the factor $(\pi^{1/2}v_{\rm th}^-)^{-1}\exp[-(v/v_{\rm th}^-)^2]$ in the final formulas (16) and (19) by $g_0^-(v)\equiv 2\pi\int_0^\infty sf_0^-(s^2+v^2)ds(\int_{-\infty}^{+\infty}g_0^-dv=1)$. Finally, we can also generalize our results to a slab geometry. Experimentally, one can create a negative ion density depletion in a slab by using a thin flat laser beam. It is easy to show that, for this case, our expressions (16) and (19) still hold (of course, r must be replaced by the distance x from the midplane), but Ψ is simplified significantly and becomes

$$\Psi(x,a)=\Delta(x-a)/n_0^-\ . \tag{20}$$

III. EXAMPLES AND DISCUSSION

In this section we shall consider various applications of our theory. The presentation will be separated into two parts. In the first part we shall study the simplest slab geometry case, but not necessarily limit ourselves to a specific negative ion velocity distribution function. In the second part, we shall consider the cylindrical case with a Maxwellian distribution of the H^- ions. That case will be used as a model for interpreting previous experimental results [7].

A. The slab geometry

We proceed from analyzing the evolution of the H^- ion density perturbation in the slab geometry for a general normalized distribution $g_0^-(v)$. In this case Eq. (19) yields (see the discussion at the end of the previous section)

$$\delta n^-(x,t)/n_0^-=-2(n_0^-)^{-1}\int_0^{+\infty}\Delta(x-vt)g_0^-(v)dv\ . \tag{21}$$

Now, we consider the case when the intensity of the laser light is sufficiently high so that all the negative ions are destroyed in a plasma layer of thickness $2d(|x|<d)$. Then one can use a square step function for Δ, i.e.,

$$\Delta(x)=\begin{cases}n_0^-, & |x|\le d\ ,\\ 0, & |x|>d\ ,\end{cases} \tag{22}$$

allowing one to rewrite (21) as

$$\delta n^-(x,t)/n_0^-=-2\int_{x/t}^{(x+d)/t}g_0^-(v)dv\ . \tag{23}$$

Next we consider the evolution of $\delta n^-(x,t)/n_0^-$ at the plane of symmetry ($x=0$):

$$\delta n^-(0,t)/n_0^-=-2\int_0^{+d/t}g_0^-(v)dv\ . \tag{24}$$

We see that $|\delta n^-(0,t)|/n_0^-$ is a decreasing function of time. Asymptotically, for $d/t\ll v_{\rm th}^-$ we obtain $\delta n^-(0,t)/n_0^-=-(2d/t)g_0^-(0)$. It is also interesting to observe that, if we define $\xi=d/t$, then, on differentiating (24), we obtain

$$(d/d\xi)[\delta n^-(x,t)/n_0^-]=-2g_0^-(\xi)\ . \tag{25}$$

On the other hand (see the end of Sec. II),

$$g_0^-(\xi)=\pi\int_0^\infty f_0^-(s^2+\xi^2)ds^2=\pi\int_{\xi^2}^\infty f_0^-(p)dp\ . \tag{26}$$

By differentiating (25), we find

$$(d^2/d\xi^2)[\delta n^-(x,t)/n_0^-]=4\pi\xi f_0^-(\xi^2)\ . \tag{27}$$

Thus, there exists a possibility for the experimental determination of the velocity distribution $f_0^-(v^2)$ of the negative ions by measuring the time evolution of the density of H^- at the symmetry plane in the slab geometry and calculating the appropriate second derivative with respect to ξ. The method is reminiscent of the electrostatic probes for measuring the electron velocity distributions in weakly ionized plasmas [8]. At large distances from the illuminated region ($x\gg d$) the asymptotic ($d/t\ll v_{\rm th}^-$) evolution of the negative ion density is also

simple, i.e., $\delta n^-(x,t)/n_0^- \approx -(2d/t)g_0^-(x/t)$. This result suggests another way of measuring the H^- velocity distribution.

At this point we proceed to the analysis of the evolution of the density perturbations of other plasma species in the slab geometry at the midplane ($x=0$) and, to be concrete, assume the Maxwellian distribution of H^-. In this case, Eq. (16) yields

$$\frac{\delta n^e(0,t)}{n_0^-} = 2\int_0^{+\infty} \frac{[v_a^2-(v_{\rm th}^+)^2]\Delta(v_a t)-[v^2-(v_{\rm th}^+)^2]\Delta(vt)}{n_0^-(\pi^{1/2}v_{\rm th}^-)[v_a^2-v^2]} \exp[-(v/v_{\rm th}^-)^2]dv \ . \tag{28}$$

Since, at present, there is no experiment in slab geometry, we illustrate our theory by a numerical example presented in Fig. 2. The solid lines in Fig. 2(a) show the dependence of the relative electron density perturbation $\delta n^e(0,t)/n_0^-$ on the dimensionless "time" $\tau = v_{\rm th}^- t/d$, for five different values of the ratio $\alpha=(\gamma T^+/T^e)^{1/2}$ (0, 0.25, 0.5, 0.75, and 1). We have assumed $M^+(v_{\rm th}^-)^2/k_B T^e=1$ in these examples and used a modified square step function with a smooth boundary for the initial electron density perturbation,

$$\Delta(x)=n_0^-\{1+\exp[(x-d)/\lambda]\}^{-1} , \tag{29}$$

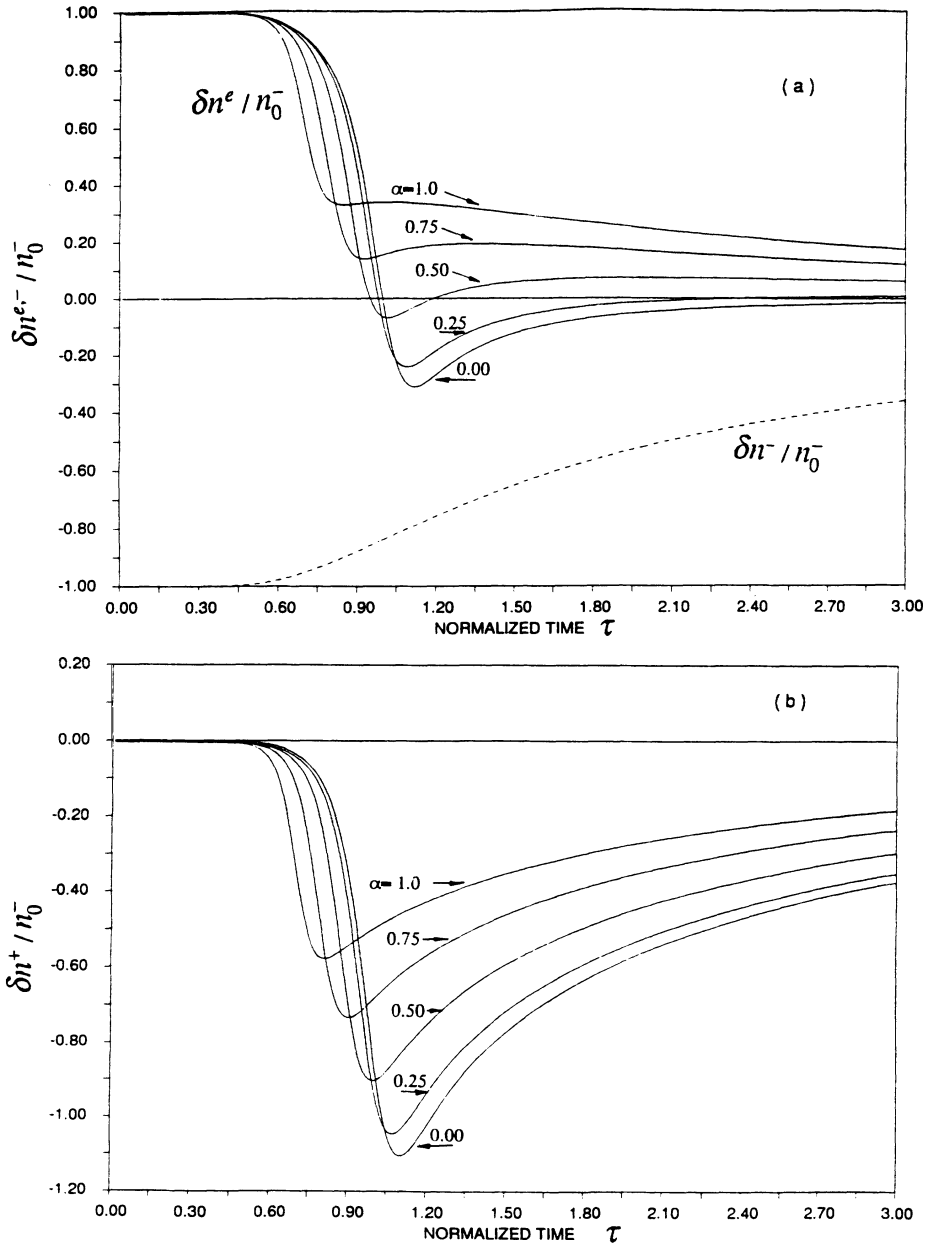

FIG. 2. Normalized density variations of different plasma species versus normalized time $\tau=v_{\rm th}^- t/d$ at the plane of symmetry in the slab geometry. (a) $\delta n^e/n_0^-$ (solid lines) and $\delta n^-/n_0^-$ (dashed line); (b) $\delta n^+/n_0^- = (\delta n^e+\delta n^-)/n_0^-$. In these examples $M^+(v_{\rm th}^-)^2/k_B T^e=1$, $\lambda/d=0.05$, and values of $\alpha=\sqrt{\gamma T^+/T^e}$ are shown by numbers.

where λ ($\lambda/d=0.05$ in our examples) measures the width of the transition region and must be at least several Debye lengths to be consistent with the plasma approximation. The dashed line in Fig. 2(a) represents the relative density variation $\delta n^-(0,t)/n_0^-$ of H^-. Finally, the relative positive ion density perturbations $\delta n^+(0,t)/n_0^-$ corresponding to the five cases in Fig. 2(a) are shown in Fig. 2(b). We can see in the figures that, for small values of α, the τ dependence of the electron density perturbation exhibits a characteristic overshoot in the vicinity of $\tau=v_{th}^-/v_a$. Physically, this overshoot is due to the two ion acoustic wave forms propagating from the boundaries of the illuminated region ($x=\pm d$) to the midplane. These wave forms "collide" at $\tau\approx v_{th}^-/v_a$ (i.e., $t\approx d/v_a$) and, formally, for $\lambda\to 0$ [when the integrand in (26) is singular at $v=v_a$] one obtains an infinite negative value of $\delta n^e(0,t)/n_0^-$ at $t=d/v_a$. In practice, however, the nonlinearities, the Debye shielding, the effect of the electric field on the negative ion kinetics (phenomena neglected in this work), or finite values of λ (as in the examples in Fig. 2), may limit the size of the overshoot. When α increases (say, due to the decrease of T^e), the ambipolar potential, driven by the electron thermal motion, decreases, the positive ion fluid becomes increasingly motionless, and the overshoot in $\delta n^e(0,t)/n_0^-$ decreases [see Fig. 2(b)] and even disappears, for large α, as the electron density follows more closely that of the negative ions.

B. The cylindrical geometry

In principle, all the physical phenomena described above and, in particular, the creation of the overshoot in the electron density on the axis of symmetry, the decrease of the ambipolar potential with the decrease of the electron temperature, etc., remain similar to those in slab geometry. Nevertheless, the cylindrical case is more complicated because of the geometric focusing effects leading to a more complex formula for Ψ [see Eq. (18)]. Therefore, we proceed from finding an expression for Ψ on the axis of symmetry ($r=0$) for the simplest model of the initial electron density perturbation,

$$\Delta(r)=\begin{cases} n_0^-, & r\le R\ , \\ 0, & r>R\ . \end{cases} \tag{30}$$

This case allows the analytic [9] evaluation of (18)

$$\Psi(0,a)=\begin{cases} -1, & a\le R\ ; \\ [(a/R)^2-1]^{-1/2} & \\ \times\{(a/R)+[(a/R)^2-1]^{1/2}\}^{-1}, & a>R\ , \end{cases} \tag{31}$$

or, by defining the auxiliary variable s via $a/R\equiv\cosh(s)$,

$$\Psi(0,a)=\begin{cases} -1, & a\le R\ , \\ [e^s\sinh(s)]^{-1}, & a>R\ \ (s>0)\ . \end{cases} \tag{32}$$

At this stage, we use (32) for finding the time evolution of the negative ion density perturbation on the axis. This evolution is already known from previous studies [5], and will serve as a check of our theory. Thus, we substitute (32) into (19)

$$\delta n^-(0,t)/n_0^- = -2(\pi^{1/2}v_{th}^-)^{-1}\left\{\int_0^{R/t}\exp[-(v/v_{th}^-)^2]dv-\int_{R/t}^{\infty}\frac{\exp[-(v/v_{th}^-)^2-s]}{\sinh(s)}dv\right\}, \tag{33}$$

where $vt/R\equiv\cosh(s)$. We can rewrite (33) as

$$\delta n^-(0,t)/n_0^- = -2(\pi^{1/2}v_{th}^-)^{-1}\left\{\int_0^{\infty}\exp[-(v/v_{th}^-)^2]dv-\int_{R/t}^{\infty}\frac{\exp[-(v/v_{th}^-)^2]}{\tanh(s)}dv\right\}. \tag{34}$$

The second integral in (34) is evaluated easily by transforming $\tanh(s)$ back to the v variable. The final result is

$$\delta n^-(0,t)/n_0^- = -\{1-\exp[-(R/v_{th}^-t)^2]\} \tag{35}$$

and, therefore, the H^- density on the axis evolves as $n^-(0,t)=n_0^-\exp[-(R/v_{th}^-t)^2]$, in agreement with the previous result [5].

Next, we consider the evolution of the electron density perturbation on the axis. We start again from a numerical example. In order to avoid the singularity in (31) associated with the assumption of a sharp initial density perturbation profile at $r=R$, we shall use the following smooth modification for Ψ:

$$\Psi(0,a)=\begin{cases} 1-2/\{1+\exp[(a-R)/\lambda]\}, & a\le R\ , \\ \left[(a/R)^2-1+\dfrac{2(\lambda/R)^2(a/R+1)}{(a/R-1)^2}\right]^{-1/2} & \\ \times\{(a/R)+[(a/R)^2-1]^{1/2}\}^{-1}, & a>R\ . \end{cases} \tag{36}$$

For sufficiently small values of λ, this function is a good approximation to (32) for all a but in a small transition region $|a-R|/\lambda\sim 1$. At the same time, (36) is continuous at $a=R$ [$\Psi(0,0)=0$] and has a continuous first derivative $\partial\Psi/\partial a=1/2\lambda$ at this point. Figure 3 shows the dependence of the electron density perturbation on the normalized time $\tau=tv_{th}^-/R$, as obtained by evaluating (16) numerically by using (36). We have again assumed that $v_{th}^-=(k_BT^e/M^+)$, used $\lambda/R=0.1$, and presented the results for five values of the parameter $\alpha=\sqrt{\gamma T^+/T^e}$ (0, 0.25, 0.5, 0.75, and 1). The dashed line in the figure shows the density recovery curve for the H^- ions [see Eq. (35)] in this example. By comparing these results with those in Fig. 2 for the slab geometry, we conclude that all the general features of the evolution in both cases are similar, but the recovery of the negative ion density is faster and the size of the electron density overshoot is larger in the cylindrical geometry. Both these effects can be explained by the focusing in the cylin-

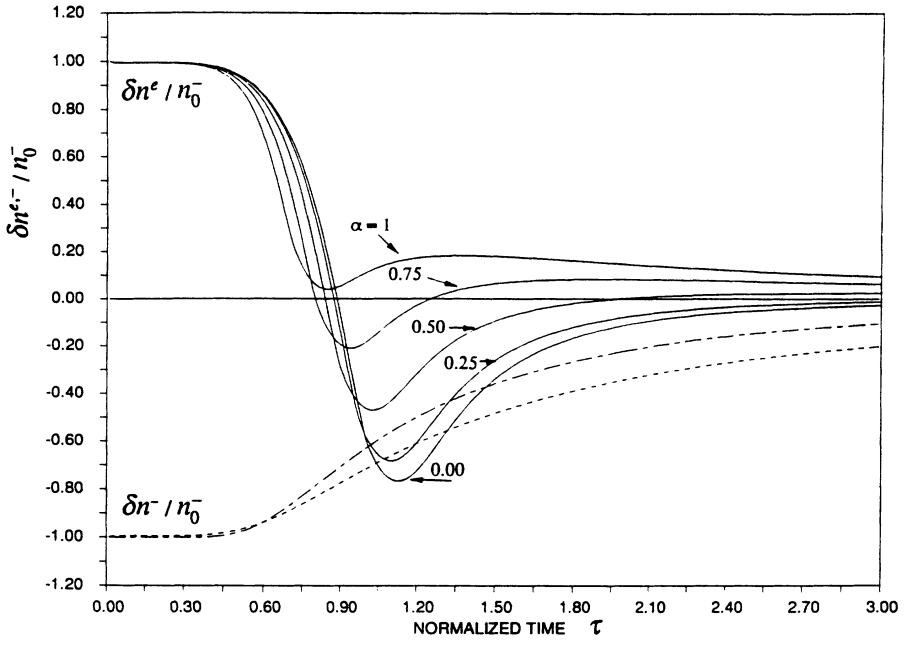

FIG. 3. Normalized density variations $\delta n^e/n_0^-$ (solid lines) and $\delta n^-/n_0^-$ (dashed line) on the axis of symmetry in the cylindrical geometry versus normalized time $t=v_{\text{th}}^- t/R$. In these examples $M^+(v_{\text{th}}^-)^2/k_B T^e = 1$, $\lambda/R=0.1$, and the values of $\alpha=\sqrt{\gamma T^+/T^e}$ are shown by numbers. The dot-dashed line represents the negative ion recovery curve given by the ballistic theory [5] with $\lambda/R=0$.

drical geometry. We also observe in the figure, as in the slab geometry, the rapid disappearance of the electron density overshoot with increase of the positive ion temperature. The explanation of this phenomenon is the same as given above in the slab case. Thus, we conclude that the analysis of the electron density overshoot following a fast photodetachment pulse can provide useful information on the relative values of the electron and positive ion temperatures. Finally, in Fig. 3, we added the negative ion density recovery curve (the dot-dashed line) predicted by the ballistic theory in the case $\lambda/R=0$. We see that a finite value of λ yields a slower recovery. The slowing down of the negative ion density return to the steady state at later times, as compared to that predicted by the ballistic theory [5], (which assumed $\lambda/R=0$) has been observed in experiments [6] and explained by such factors as collisions and self-consistent electric fields. Thus, now, we suggest an additional possibility.

As the final application of the theory, we shall interpret our previous measurements [7] of the ratio $\rho=\delta n^e(0)/|\delta n^e_{\min}|=n_0^-/|\delta n^e_{\min}|$ between the initial electron density increase on the axis and the magnitude of the electron density overshoot versus the laser beam diameter $D_L=2R$. These measurements were performed in the hybrid multicusp ion source described in Refs. [4] and [6] and are presented in Fig. 4. We can see in the figure that at the largest laser beam diameter ($D_L=1.2$ cm), $\rho\approx 2$. As the laser diameter decreases, the relative size of the overshoot first increases and reaches that of the maximum of the probe signal ($\rho\approx 1$), but later ρ increases again with decrease of D_L. We can explain this characteristic behavior as follows. The laser beam diameter in these experiments was controlled by masking the outer and less intense part of the beam. This led to sharper edges of the initial electron (negative ion) density perturbations as D_L decreased. The sharpening process took place until saturation of the photodetachment efficiency at the edge of the laser beam. This phenomenon can be modeled in our theory by varying the width λ of the transition region in (34) relative to the beam radius R. The results of such calculations for the parameters of Fig. 3 (the $\alpha=0.5$ case), but several values of λ/R are presented in Fig. 5. We see in this figure that the values of $\rho=n_0^-/|\delta n^e_{\min}|$ found in these calculations are in the range of the experimental results in Fig. 4. We also see that decrease of λ/R leads to a decrease of ρ. Thus, one can explain the characteristic minimum in Fig. 4 by the competition between the values of λ and R in the ratio λ/R. Both parameters decreased with decrease of the laser beam diameter, but, if initially λ decreased faster, then λ/R and therefore ρ decreased, while later, after saturation, as R decreased, λ remained fixed, and both λ/R and ρ increased rapidly.

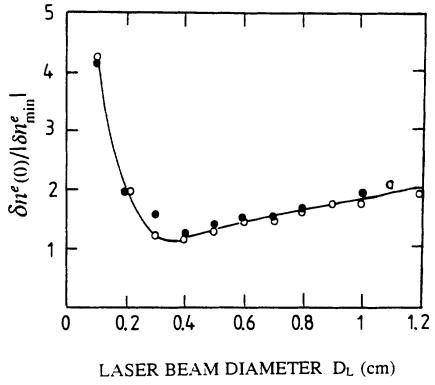

FIG. 4. Measured [7] ratio $\rho=\delta n^e(0)/|\delta n^e_{\min}|=n_0^-/|\delta n^e_{\min}|$ between the initial electron density increase on the axis after the laser pulse and the magnitude of the electron density overshoot versus the laser beam diameter D_L.

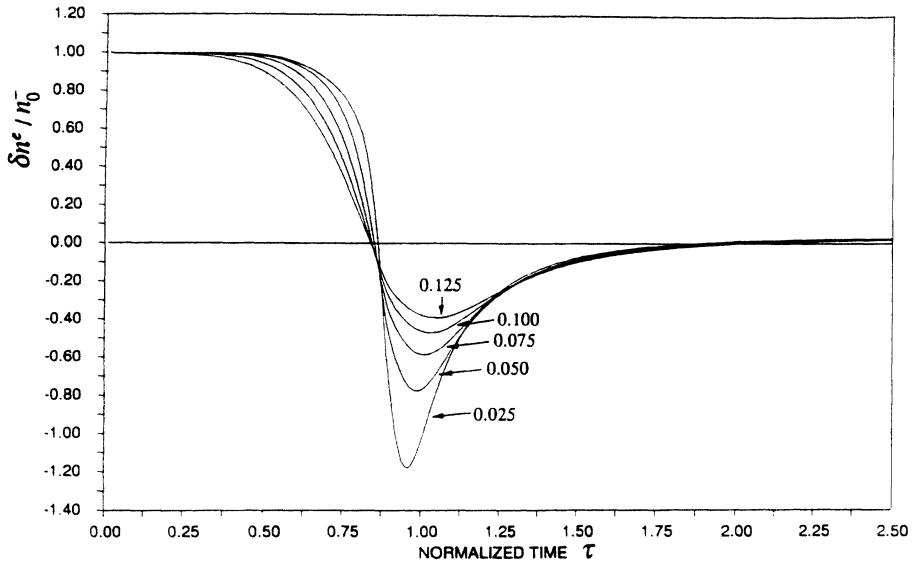

FIG. 5. Normalized electron density perturbation $\delta n^e/n_0^-$ on the axis in the cylindrical geometry versus normalized time $\tau=v_{th}^- t/R$. In these examples $M^+(v_{th}^-)^2/k_B T^e=1$, $\alpha=\sqrt{\gamma T^+/T^e}=0.5$, and the values of λ/R are shown by numbers.

IV. CONCLUSIONS

(i) We have analyzed theoretically the space-time evolution of various plasma components in photodetachment experiments in negative ion plasmas. The plasma was described by a hybrid, fluid-kinetic, three-species (electrons, H^-, and H_3^+ ions) model. We used a fluid description for the electrons and the positive ions, while the negative ions were represented by a "ballistic" kinetic model, where one neglects the effects of the electric field. It was shown that this approximation is justified in plasmas where the negative ions are the minority species and $T^- \sim O(T^e)$.

(ii) We have considered two possible experimental geometries, i.e., the slab and the cylindrical cases. Analytic solutions for the densities of all three plasma species in the electric field in space and time were found for both geometries. The simpler slab case (not yet exploited experimentally) yields the possibility of experimental deduction of the negative ion velocity distribution by measuring the time dependence of the negative ion density at the symmetry plane.

(iii) We have explained the experimentally observed characteristic overshoot of the electron density perturbation at the symmetry axis in the cylindrical geometry. A similar effect is also characteristic of the slab geometry, but the overshoot in the cylindrical case is more pronounced due to the geometric focusing effect. Because of the overshoot, the evolution of the electron component on the axis differs significantly from a smooth (nonoscillatory) return of the negative ions to the steady state. This anomaly in the electron density evolution is due to the motion of (initially unperturbed) positive ions under the action of the self-consistent electric field, caused by the thermal motion of the electrons and the nonuniformity. The motion of the ion fluid is significant only in the presence of a sufficiently strong electric field, so that the ratio between the electron and positive ion temperatures plays an important role in determining the size of the overshoot. If the electron temperature is much less than that of the positive ions, the positive ions remain almost stationary. As a result, the overshoot disappears and the electron density evolution follows that of the negative ions to preserve quasineutrality. Thus, measurements of the relative size of the overshoot may serve as a diagnostic tool for the determination of T^e and T^+ in future experiments.

(iv) The theory predicted increase of the relative size of the electron density overshoot (on the axis) with the ratio λ/R where λ is the spatial width of the transition region from low to high negative ion densities at the edge of the laser beam and R is the radius of the beam. When λ decreases the size of the overshoot increases and, formally, becomes infinite in the limit $\lambda=0$ at a time equal to the transition time with the ion acoustic speed from the edge to the axis. In practice, however, nonlinear effects, Debye shielding, and the effect of the electric field on the negative ion kinetics (phenomena not included in this study) may saturate the size of the overshoot. Thus, the analysis of this "singularity" in negative ion plasmas is an interesting goal for future studies.

ACKNOWLEDGMENTS

One of the authors (L.F.) acknowledges Ecole Polytechnique and the PMI laboratory for providing the excellent environment for this research during the sabbatical leave from the Hebrew University of Jerusalem.

[1] W. S. Cooper, Phys. Fluids B **4**, 2300 (1992).
[2] See, for example, the reviews G. W. Hamilton and M. Bacal, IEEE Trans. Plasma Sci. **19**, 1143 (1991); A. J. T. Holmes, Plasma Phys. Controlled Fusion **34**, 653 (1992).
[3] M. Bacal, G. Hamilton, A. M. Bruneteau, H. J. Doucet, and J. Taillet, Rev. Sci. Instrum. **50**, 719 (1979).
[4] P. Devynck, J. Auvray, M. Bacal, P. Berlemont. J. Bruneteau, R. Leroy, and R. A. Stern, Rev. Sci. Instrum. **60**, 2873 (1989).
[5] R. A. Stern, P. Devynck, M. Bacal, P. Berlemont, and F. Hillion, Phys. Rev. A **41**, 3307 (1990).
[6] M. Bacal, P. Berlemont, A. M. Bruneteau, R. Leroy, and R. A. Stern, J. Appl. Phys. **70**, 1212 (1991).
[7] M. Bacal, J. Brunetau, P. Devynck, and F. Hillion, PMI Report No. 1891, Ecole Polytechnique, 1987 (unpublished).
[8] Yu. M. Kagan and V. I. Perel, Usp. Fiz. Nauk, **81**, 409 (1963) [Sov. Phys. Usp. **6**, 767 (1964)].
[9] *Handbook of Mathematical Functions,* edited by M. Abramowitz and I. A. Stegun (Dover, New York, 1972), pp. 484, 487.